

Capture and extraction of phenotypic traits from novel high-density point clouds

Robin Hartley, Sadeepa Jayathunga, Peter Massam, Sam Davidson, Dilshan De Silva, Honey Jane Estarija, Adedamola Wuraola, Grant Pearse.



Date: 25.11.2021

Report No: RFP-T014

TABLE OF CONTENTS

Executive Summary	1
1. Introduction	2
2. Materials	3
2.1. Study Site.....	3
2.2. Field Data.....	4
2.3. Ground control: CloudReg.....	5
2.4. UAV Data	6
2.5. MLS Data	6
3. Methodology	8
3.1. Processing raw data.....	8
3.1.1. MiniVUX.....	8
3.1.2. Hovermap.....	8
3.2. Point cloud processing and analysis.....	8
3.3. Derived metrics	8
3.4. Deep learning segmentation methodology.....	10
3.5. Accuracy Statistics	10
4. Results	11
4.1. Tree stem segmentation using deep learning	11
4.2. Diameter at breast height	12
4.3. Tree height prediction.....	12
4.4. Stem volume	14
4.5. Whorl detection	14
5. Discussion.....	15
5.1. Tree stem segmentation using deep learning	15
5.2. Diameter at Breast Height	16
5.3. Height.....	17
5.4. Stem Volume.....	18
5.5. Whorl Detection.....	18
6. Conclusions	19
Acknowledgements.....	19
Glossary	20
References	22

Disclaimer

This report has been prepared by New Zealand Forest Research Institute Limited (Scion) for Forest Growers Research Ltd (FGR) subject to the terms and conditions of a research fund agreement dated 1 April 2014.

The opinions and information provided in this report have been provided in good faith and on the basis that every endeavour has been made to be accurate and not misleading and to exercise reasonable care, skill and judgement in providing such opinions and information.

Under the terms of the Services Agreement, Scion's liability to FGR in relation to the services provided to produce this report is limited to the value of those services. Neither Scion nor any of its employees, contractors, agents or other persons acting on its behalf or under its control accept any responsibility to any person or organisation in respect of any information or opinion provided in this report in excess of that amount.

EXECUTIVE SUMMARY

Phenotyping has been a reality for aiding the selection of optimal crops for specific environments for decades in a number of horticultural industries. Until recently, phenotyping for forest managers and tree breeders has been difficult due to the size of the crop and the length of rotation making measurement and study difficult. With the advent of affordable, accurate and non-destructive technologies, phenotyping is becoming a reality for forestry. These tools must now be refined and harnessed to benefit forestry.

In this study, two novel, high-density laser scanners are assessed for their ability to derive phenotypic measurements from a mature stand of *Pinus radiata*. Mobile laser scanning (MLS) under the forest canopy and UAV laser scanning (ULS) above the forest canopy are combined and contrasted to assess their efficacy in deriving tree form measurements including tree height, diameter at breast height, stem volume, and whorl detection. Deep learning-based methods are also assessed as a means of streamlining the delineation of individual trees.

The findings of this study indicate that the technology shows strong potential for increasing throughput for phenotyping platforms. A key finding of this study has been that, from the ground, MLS is able to derive canopy heights at a comparable level of precision and accuracy to a high-end ULS scanner from the air ($R^2 = 0.94$, RMSE = 3.02%), negating the need for capturing above-canopy data to obtain accurate tree heights and canopy height models. We also observed strong agreement between field measurements and MLS-derived estimates of stem volume ($R^2 = 0.99$, RMSE = 10.16% and DBH $R^2 = 0.90$, RMSE = 9.95%).

Our findings indicate that ULS is less useful for the characterisation of stem form; however, deep learning methods to delineate individual trees from ULS data show promise for characterising these attributes in the future.

Overall, the work presented in this technical note demonstrates that these technologies hold strong potential for advancing tree measurement practices in forestry, with exciting implications for phenotyping our forests.

1. INTRODUCTION

Digital phenotyping is an emerging science that uses non-invasive techniques such as laser scanning to assess the interaction between genetics, environmental factors and silviculture (GxExS) to guide the selection of the most productive trees for a given environment (Costa, et al., 2018). In forestry, phenotyping is emerging as a means of selecting the right tree, for the right place, for the right purpose, and to increase the efficiency of tree breeding programmes (Dungey, et al., 2018). Current phenotyping methodologies require the combination of GxExS data with the physical description of tree form (Pont, et al., 2020). The traditional methods for the physical description of tree form are manual, time-consuming, costly, and error-prone, severely limiting the throughput (Bombrun, et al., 2020; Dungey, et al., 2018).

Remote sensing is a useful tool for in situ tree phenotyping, with data from sources that include airborne laser scanning (ALS) being useful for deriving information such as slope, aspect, and geographical location (Pont, et al., 2020). ALS has been researched extensively for tree height assessment, stand density and crown metrics (Hartley, et al., 2020; Pearse, et al., 2019; Pont, 2016; Pont, et al., 2020; Watt, et al., 2014). However, ALS is limited in its ability to describe stem form. The heavy occlusion caused by the dense forest canopy and the lower pulse density of ALS provides extremely sparse characterisation of the tree stems that make it unsuitable for comprehensive tree form assessment (Windrim, et al., 2020).

Alternate methods for the description of tree form have largely been focused on terrestrial laser scanning (TLS). Statically-mounted TLS has been explored for forestry applications for nearly two decades (Hopkinson, et al., 2004; Lovell, et al., 2003; Thies, et al., 2004; Watt, et al., 2005). Research has focused on topics such as scanning forestry plots, deriving tree form metrics and assessing the efficacy of TLS as a tool for carrying out forest inventory (Abegg, et al., 2017; Kankare, et al., 2014; Liang, et al., 2016; Mengesha, et al., 2015; Newnham, et al., 2015; Raunonen, et al., 2015). This research has shown that TLS is capable of very accurate measurement of tree form metrics (Liang, et al., 2016) but the technology has not seen broad operational use due to the impractical nature of capturing and aligning multiple scans from a static scanner to achieve plot-level coverage (Newnham, et al., 2015). TLS also produces less stem returns from the upper stem due to occlusion from branching (Liang, et al., 2018). This can also lead to reduced accuracy in height measurement if the tree tip is occluded (Cabo, Del Pozo, et al., 2018).

Mobile laser scanning (MLS) as an alternate technology to TLS has been developed for forest environments since 2013 (Holopainen, et al., 2013). These systems are similar to ALS, in that they combine a laser scanner with an inertial measurement unit (IMU) and global navigation satellite system (GNSS) onto a moving platform (Bauwens, et al., 2016). Arguably it was not until the GNSS component was replaced with simultaneous localisation and mapping (SLAM) algorithms that these systems became truly suited to the forest environment. SLAM algorithms are GNSS-independent and enable the creation of spatially accurate point clouds in GNSS-denied environments such as beneath a forest canopy. These more lightweight MLS systems are often referred to as personal, handheld or backpack laser scanners depending on the configuration of the unit. In recent years there has been a growing body of research focused on MLS application within forestry (Bauwens, et al., 2016; Cabo, Del Pozo, et al., 2018; Holopainen, et al., 2013; Hyypä, et al., 2020; Ryding, et al., 2015). By their very nature, MLS systems achieve more complete coverage of a forest environment in a shorter timeframe, addressing the issues that make TLS impractical for forest inventory (Shao, et al., 2020). The increased mobility of these units comes at a price, however, as MLS are often restricted to integrating lightweight scanners that have large beam divergence and lower power, which limit their range and accuracy (Bienert, et al., 2018; Tang, et al., 2015), specifically when characterising the upper part of tree stems to a greater extent than TLS (Bienert, et al., 2018).

Another alternative to traditional tree form description techniques is UAV laser scanning (ULS). ULS takes advantage of the miniaturisation of airborne laser scanning technology in recent years, allowing for close-range aerial captures over forested areas with much higher pulse densities. ULS systems vary in their accuracy depending on the scanner utilised, with high-end options including

the Riegl VUX range, and more affordable options utilising re-purposed automotive laser scanners, such as the Velodyne Puck range (Kellner, et al., 2019). As with ALS, ULS still suffers from the same occlusion issues caused by the forest canopy. However, owing to the closer range, and vastly increased pulse density, stem characterisation methods for TLS data have been effectively adapted to ULS data (Bruggisser, et al., 2020; Hyyppä, et al., 2020; Torresan, et al., 2020).

Algorithms for tree form description from point clouds have been developed for a range of metrics including tree stem segmentation (Zhang, et al., 2019), diameter at breast height DBH (Bu, et al., 2016), stem straightness (Mengesha, et al., 2015), stem volume (Buck, et al., 2019), and branch characterisation (Boudon, et al., 2014). The majority of these algorithms work on heuristic principles, or what can be thought of as “traditional algorithms”. Increasingly, machine learning and especially deep learning (DL) are being applied to TLS data. Studies have been devoted to the application of DL for individual tree crown delineation, stem delineation and stem volume from TLS and even ALS point clouds (Braga, et al., 2020; Windrim, et al., 2019; Windrim, et al., 2020; Xi, et al., 2018).

This tech note presents the results from a comparison of tree form metrics derived from MLS and ULS data utilising various algorithms with traditional field measurements. The traditional measurements are considered to be the baseline for this study. The results of this study will then be discussed with relevance to the applicability of these tools in the context of commercial forestry.

2. Materials

2.1. STUDY SITE

The study site selected for this research was a genetics trial archive located in the Scion nursery in Rotorua (Figure 1). The trial stand was approximately two hectares in size and comprised *Pinus radiata* D. don with an age range of eighteen to twenty years. Details of the tree size in the trial can be found in Table 1 and Figure 2.

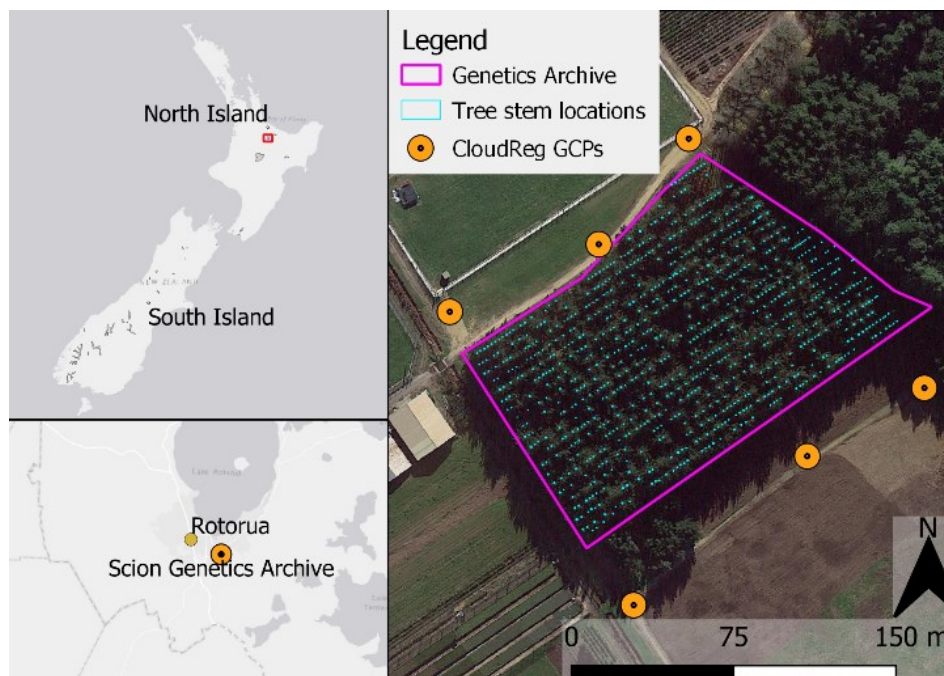


Figure 1. Map of the study site showing the area of the trial stand (purple box) and the locations of tree stems in the study (blue polygons). Insets show location of trial site in relation to the Rotorua region and New Zealand (NZ).

Table 1. Table showing height and diameter distributions of the studied trees with mean and standard distribution (in brackets).

No. Trees	DBH Range (cm)	Mean DBH (SD) (cm)	Height Range (m)	Mean Height (SD) (m)
884	2.2-67.1	34.65 (12.81)	1.7-34.4	23.9 (7.93)

The stand is located on a very flat site and is regularly mowed for access. Consequently, it has very little understory, which is limited to small patches of low-growing blackberry between the lines of trees. The aim of this study was to assess the absolute accuracy of phenotypic measurements from laser-scanned point clouds against field measurements. This site was, therefore, an ideal choice for this study, providing idealised conditions with little noise from understory or terrain undulations to confound the measurements.

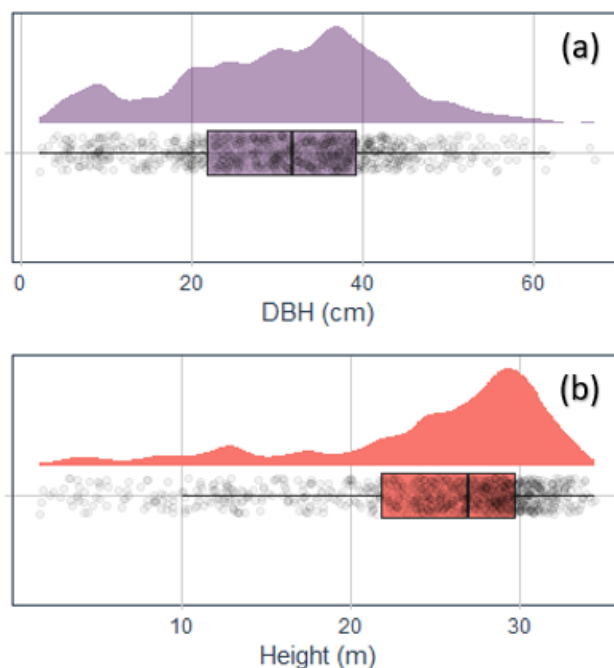


Figure 2. Plots showing distribution of diameter (a) and height (b) for the 884 trees in this study.

2.2. FIELD DATA

Ground validation for this study was carried out in the form of traditional forest mensuration. Pre-harvest inventory (PHI) was conducted on every tree within the stand following the PlotSafe methodology and utilising the RAD05 cruising dictionary (CNI Regional YTGEN User Group, 2007). Phenotypic traits were measured at the tree level and included DBH measured at 1.4 m, tree height, stem straightness, branch size, green crown height, and stem malformation. PHI was conducted between the 12th and 16th October 2020. Due to the time elapsed between field measurements and laser scanning, remeasurement of DBH was carried out between the 11th and 13th August 2021.

In addition to the mensuration data, a sub-sample of twelve trees were intensively measured using a crown mapping procedure. For this exercise, more intensive phenotypic measurement was undertaken for selected trees including measurements of internodal diameters, internodal distances, whorl height above ground level (AGL) and branch diameters for the entire stem up to a height of 20 m. This involved a crew of two certified climbers climbing each tree to collect measurements. Heights and internodal measurements were measured with a 50 m nylon measuring tape that was secured at the base of the tree and in the tree crown (Figure 3). Internodal diameters were measured with a DBH tape and branch diameters were measured with electronic Vernier callipers with an accuracy of 0.2 mm.



Figure 3. Image showing measurements being recorded to a mobile application during crown mapping.

2.3. GROUND CONTROL: CLOUDREG

Aligning the inventory measurements with field measurements in mature forestry trials is traditionally a difficult exercise owing to the low accuracy of GNSS data captured beneath the forest canopy (Dash, et al., 2019). Throughout the Resilient Forests programme, Scion has developed a system called CloudReg to achieve highly accurate co-registration of airborne and terrestrial remotely sensed data sets. This allows for precise plot maps, and in turn the confidence to enable tree-level comparisons of field and remotely sensed data sets.



Figure 4. Image of target deployed to the site as a ground control point.

Prior to data capture, ground control was established across the site utilising Scion's CloudReg methodology. Ground control points (GCPs) were established on paths and open ground around the perimeter of the stand (Figure 1) utilising six 1 m² targets coated in highly reflective material (Figure 4). These targets were then left on site for both the UAV and Hovermap data captures. These targets are clearly visible within all of the intensity-colourised lidar point clouds to allow for accurate co-registration of the various data sets.

Once the data had been captured and the ULS and MLS point clouds were processed, the two data sets were loaded into the CloudCompare software package (CloudCompare, version 2.12 alpha; CloudCompare, Paris, France). The point clouds were coloured by backscatter intensity values and,

using the Align (point pairs picking) tool, were co-registered by aligning the GCPs within both data sets. Hovermap data from the backpack configuration does not contain GNSS data, and therefore it is important to align the Hovermap data to the MiniVUX data, which is georeferenced.

2.4. UAV DATA

ULS data for this study were captured using a LidarUSA snoop V-series lidar system, with an integrated Riegl MiniVUX-1 UAV laser scanner (hereafter referred to as MiniVUX). MiniVUX data capture was carried out using a DJI Matrice 600 Pro hexacopter (DJI Ltd., Shenzhen, China).

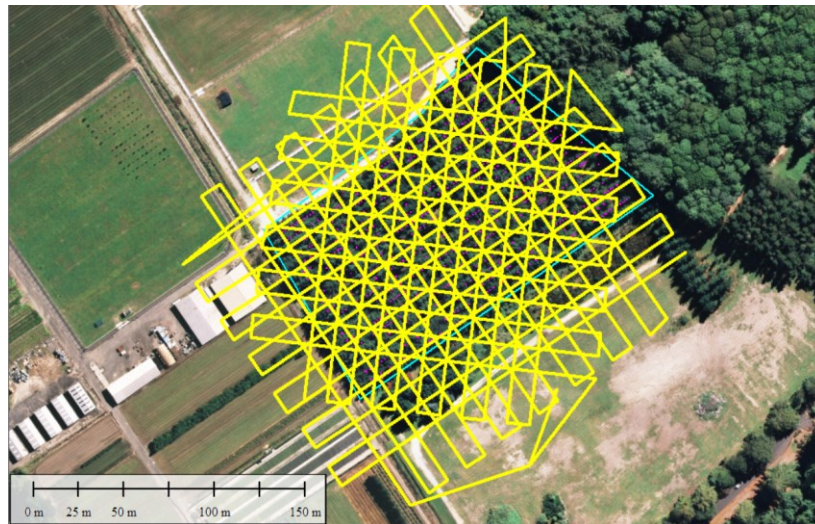


Figure 5. Flight plan for MiniVUX data capture was planned in four directions to achieve optimal coverage throughout the stand.

Flight planning was undertaken using the UgCS flight controller software (SPH Engineering, Riga, Latvia). In order to maximise point coverage throughout the stand, a flight plan was created to maximise point density. In line with recommendations from Wallace, et al. (2012), flights were carried out at 55 metres AGL to ensure a 20 m vertical separation between the tallest tree in the stand and the craft, whilst ensuring minimal beam divergence and higher point accuracy. The stand was flown in four directions with a 10-metre line-spacing between flight passes to increase pulse density and incidences of pulses penetrating gaps in the canopy. The first flight plan included flights both along and perpendicular to the rows of trees. This flight plan was then duplicated and rotated by 45° to create the second flight plan (Figure 5). MiniVUX data was captured on the 5th May 2021 and the resulting point cloud had an average pulse density of 1818 pulses per square metre (ppm²).

2.5. MLS DATA

Ground-based lidar data were captured using the Hovermap mobile laser scanner (MLS) (Emesent, Milton, QLD, Australia). The Hovermap comprises a Velodyne Puck-LITE (VLP-16) laser scanner, which houses an array of 16 lasers that spin 360° about a single axis. The scanner is also mounted on a rotating arm, which allows the whole scanner to rotate about 360° on a perpendicular plane giving the unit full spherical 360° coverage while the system is in a stationary position. The system is SLAM-based, enabling capture of coherent point clouds below the canopy independent of GNSS signal availability. The Hovermap can be utilised in multiple formats, as a handheld, backpack, vehicle-mounted or UAV-mounted MLS system. When integrated with a UAV, the Hovermap can simultaneously collect data and act as an advanced collision avoidance system for the craft it is mounted to. These collision avoidance strategies can be further broken down into two key modes: autonomy levels 1 and 2 (AL1, AL2). In AL1 mode the pilot flies the craft manually with the Hovermap enabling collision avoidance and altitude lock. AL2 is a waypoint-based autonomous flight mode that utilises the Hovermap to provide detect and avoid capabilities for the craft.

To assess the practicality of the Hovermap, the stand was scanned utilising three of the scanner configurations: backpack, AL1 and AL2 models. The Hovermap was integrated with a DJI Matrice

210 (DJI Ltd., Shenzhen, China) for the AL1 and AL2 flights. To test the limitations of the scanner, a path was planned so that the Hovermap went along either side of each row of trees within the stand approximately shoulder height. To create an accurate point cloud, the SLAM algorithm requires a process of “closing the loop” in which the scanner is required to regularly revisit areas previously scanned to aid in tying new scenes to the existing point cloud. The selected flight and walking path conformed well with these specifications. The trajectory of the backpack capture plan can be found in Figure 6. The same path was followed with the AL1 and AL2 flights.

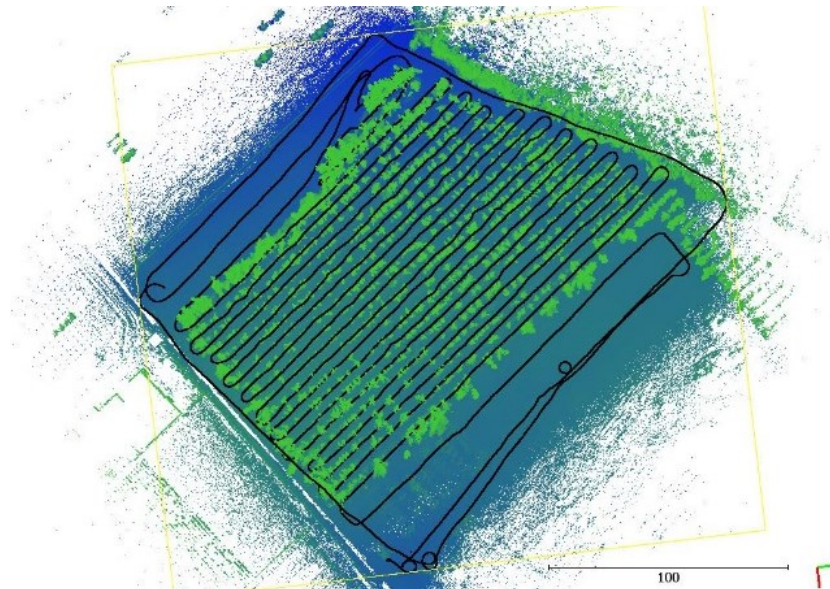


Figure 6. Trajectory of the Hovermap backpack scan (in black) overlaid on stem locations within the trial, coloured by height (blue = low, green = high).

Due to battery limitations of the craft, a total of 19 flights were required with the Hovermap in AL1 configuration to cover the site, averaging a little over one row of trees per flight (approximately 170 m). Consequently, multiple raw data files were created, which exponentially increased processing time further along the data processing pipeline. AL2 configuration utilised more battery power than AL1 and resulted in 40 raw data files, covering only half of a row per flight (approximately 85 metres). Due to these constraints, it was decided to use the backpack data set for this study, which created a point cloud with a pulse density of 22,256 ppm². Backpack data capture was carried out on the 28th July 2021. A comparison of the capture and processing constraints associated with each configuration of the Hovermap trialled can be found in Table 2.

Table 2. Table showing the capture and processing times for the assessed Hovermap configurations along with time for capture of PHI measurement.

Configuration	Time to capture (hrs:mins)	No. raw files created	Processing time (hrs:mins)	Time to merge (hrs:mins)	Total time (hrs:mins)
Backpack	0:45	1	4:00	NA	4:45
AL1	2:30	19	2:15	4:00	9:00
AL2	12:30	40	11:15	4:30	28:15
Field Inventory	36:00	NA	NA	NA	36:00

3. METHODOLOGY

3.1. PROCESSING RAW DATA

3.1.1. MINIVUX

To derive point clouds in the universal LAS data format, all ULS data were processed from the manufacturers native data formats utilising the Inertial Explorer (NovAtel Inc., Calgary, AB, Canada), and ScanLook PC (Fagerman Technologies, Inc., Somerville, AL, USA) software packages. The Snoopy V-Series system utilises a PPK (post-processed kinematic) GNSS system to enhance the accuracy of the output point clouds. As such processing involves two stages, first the GNSS rover data is post-processed utilising the data from the GNSS base station within the Inertial Explorer software. During this initial step, filtering was also applied to remove noise points within a minimum distance from the scanner. Finally, the ScanLook PC software was used to apply boresight calibration angles and lever-arm offsets to the point cloud data, removing any inherent errors.

3.1.2. HOVERMAP

Raw data files from the Hovermap were processed utilising the Emesent software package version 1.5 (Emesent, Milton, QLD, Australia). Data files were loaded into the software package, which then uses Emesent's proprietary SLAM algorithms to generate a point cloud in the LAS format. To increase the quality of matches, some parameters were adjusted from the default, including setting a spherical search radius of 1.5 m, a sliding window size of 8 seconds, and global iterations for registration set to 14.

For trials with the AL1 and AL2 Hovermap configurations, the multiple point clouds were merged using the Emesent software. There are two main methods for merging point clouds using Emesent's SLAM-based software package: one utilises the GNSS tracklog from the data capture; the other option for point clouds without a GNSS feed, involves a process of manual alignment within CloudCompare prior to merging within the Emesent software. There was sufficient GNSS data recorded below the forest canopy in this study and so the former option was utilised. Neither of the AL1 or AL2 data sets were analysed within this study, further than for the assessment of processing times (see Table 2).

3.2. POINT CLOUD PROCESSING AND ANALYSIS

Processed MiniVUX point clouds were then denoised, ground classified, and height normalised using a combination of various algorithms within the LAsTools software (Isenburg, 2019). Processed Hovermap data sets were first co-registered using Scion's CloudReg methodology. Co-registered point clouds were then put through a segmentation pipeline developed utilising multiple algorithms within the SimpleForest software package (Hackenberg, et al., 2021). The segmentation pipeline consisted of four main steps: (i) ground classification and height normalisation, (ii) stem cloud generation, (iii) individual tree segmentation, and (iv) segment post-processing. The stem cloud generated in step three was used to create a stem map of the study site, which was later validated in the field using a GIS-based mapping app and field observations.

3.3. DERIVED METRICS

The individual tree segments produced by the SimpleForest pipeline were used as inputs to a stem delineation algorithm in the TreeLS library in R (de Conto, et al., 2017). The detected stem points were then isolated and segmented into chunks using defined height intervals (5, 10 and 20 cm). Spheres were fitted to each chunk and fitting parameters, including the diameter, centre coordinates and fitting error for each sphere were calculated. The resulting diameter profiles for each individual stem were then used to derive phenotypic metrics including DBH, volume, swellings in the stem (nodes) and stem height. Individual tree point cloud processing and parameter derivation was done in R statistical software package (R Core Team, 2020).

A custom algorithm was developed in R to derive volume from the stem profiles. The algorithm fits spheres to the stem, checking first if there are enough points in each stem segment (5 /10 /15 cm) to fit a circle or sphere. If there are insufficient points, an “NA” value is assigned to that segment and the algorithm continues to the next segment. A volume calculation algorithm then combines the individual volumes of these stacked spheres moving up the stem profile into a single stem volume. The algorithm only combines consecutively stacked spheres, and so the algorithm stops combining segments when it detects an “NA” in the stem profile, even if there are additional spheres above this gap (Figure 7).

It is common practice in NZ to move the measurement of the DBH height from 1.4 m by a maximum of ± 10 cm to avoid taking the measurement over swelling. Additional guidelines are followed when moving the DBH height along the stem to ensure accuracy of measurement (CNI Regional YTGEN User Group, 2007). In accordance with these guidelines, a variable height estimation method that used stem diameter profile to detect significant changes in stem shape at every 10cm interval was instigated when extracting DBH from individual tree segments.

We used the stem diameter profile (5/10/15 cm) of each tree to detect the segments that showed a significant increase in diameter compared to their neighbouring segments and marked them as potential nodal swellings. The heights of these nodal swellings were later matched with field measured whorl heights.

Tree heights calculated from the SimpleForest pipeline displayed a strong negative bias due to aggressive noise filtering. To assess the height accuracy of each laser scanner, tree height was derived instead through a peak detection methodology. First, stem locations from the SimpleForest pipeline were used to create a shapefile of the stem locations at ground level. A buffer of 1 m was applied to each of the stem circles to create a new shapefile representing a search radius for the tree peak. Point clouds from the MiniVUX and Hovermap were then ground classified, height normalised and noise filtered to remove spurious points above the canopy using the lidR package (Roussel, et al., 2018) in R. The shapefile of potential tree peak locations was then used to calculate the maximum point height for each of the trees.



Figure 7. Image showing sphere fitting to a delineated tree stem (left), and stem points (right).

3.4. DEEP LEARNING SEGMENTATION METHODOLOGY

The use of deep learning (DL) was explored to automate stem segmentation in individual tree point clouds. Stem and foliage points from 135 MiniVUX tree point clouds were manually identified in CloudCompare as accurately as possible for use as annotations for model training. Due to the small data set size, 3-fold cross validation was implemented, with 10 trees for validation in each fold, and 8 for testing, giving a total of 24 trees to evaluate the models performance on the two classes – stem and foliage (branches and needles).

A 3D convolutional neural network Voxel 3D-FCN, which is a fusion of VoxNet (Maturana, et al., 2015) and V-net (Milletari, et al., 2016), was implemented in Forest3Dapp (Windrim, et al., 2020), and trained using the Python Tensorflow library (Abadi, et al., 2016) to segment voxels into stem and foliage. For input into Voxel 3D-FCN, individual tree point clouds are first voxelised into a 150 x 150 x 100 grid. At prediction time, the tree is voxelised and ingested by the trained model for segmentation. The K-D Tree algorithm (Bentley, 1975) is then used to map the segmented point clouds back to their original resolution by finding the nearest points.

3.5. ACCURACY STATISTICS

Statistics for precision and bias were calculated using statistical methods common to studies for the comparison of field and laser scanning metrics (Bauwens, et al., 2016; Hartley, et al., 2020) including root mean square error (RMSE) and mean bias error (MBE):

$$R^2 = \frac{\sum_i (\hat{y}_i - \bar{y})^2}{\sum_i (y_i - \bar{y})^2}$$

$$RMSE = \sqrt{\frac{\sum_{i=1}^n (\hat{y}_i - y_i)^2}{n}}$$

$$MBE = \frac{1}{n} \sum_{i=1}^n y_i - \hat{y}_i$$

where y_i represents field measurements, \hat{y}_i represents predicted measurements from point clouds, \bar{y} is the average of the observed values and n represents the sample size. The relative RMSE (RMSE%) was calculated through the expression of the RMSE as a percentage of the average observed values: $100(RMSE/\bar{y})$.

Metrics used to evaluate the per-point 3D tree segmentation accuracy were the, precision, and recall for class_i (stem and foliage) and the intersection over union (IoU) for stem segmentation:

$$Precision_i = \frac{TP_i}{TP_i + FP_i}$$

$$Recall_i = \frac{TP_i}{TP_i + FN_i}$$

$$IOU_i = \frac{Intersection}{Union} = \frac{count(y_i \cap \hat{y}_i)}{count(y_i \cup \hat{y}_i)}$$

Where TP are the number of correct predictions, FP are the number of false predictions and FN are the number of false omissions. $y_i \cap \hat{y}_i$ represents the correctly predicted point classifications for class_i and $(y_i \cup \hat{y}_i)$ represents the union of predicted and observed points for class_i, which is the summation of TP, FP, and FN. Scores for IOU range from 0 to 1 with 1 being a perfect prediction.

For assessing the accuracy of the whorl detection, percentage accuracy was calculated as per Pyörälä, et al. (2018):

$$Accuracy(\%) = \frac{n_a}{n_m + n_{fp}}$$

Where n_a represents the number of identified whorls, n_m represents the number of field measured whorls and n_{fp} represents the number of falsely predicted whorls.

4. RESULTS

4.1. TREE STEM SEGMENTATION USING DEEP LEARNING

Table 3. Table showing results of stem segmentation along with foliage and branching segmentation as IoU, precision and recall. Results displayed as mean value across all trees with standard deviation in brackets.

Tree component	IoU	Precision	Recall
Stem	0.26 (0.11)	0.27 (0.16)	0.91 (0.16)
Foliage and branching	0.84 (0.17)	0.99 (0.01)	0.85 (0.17)

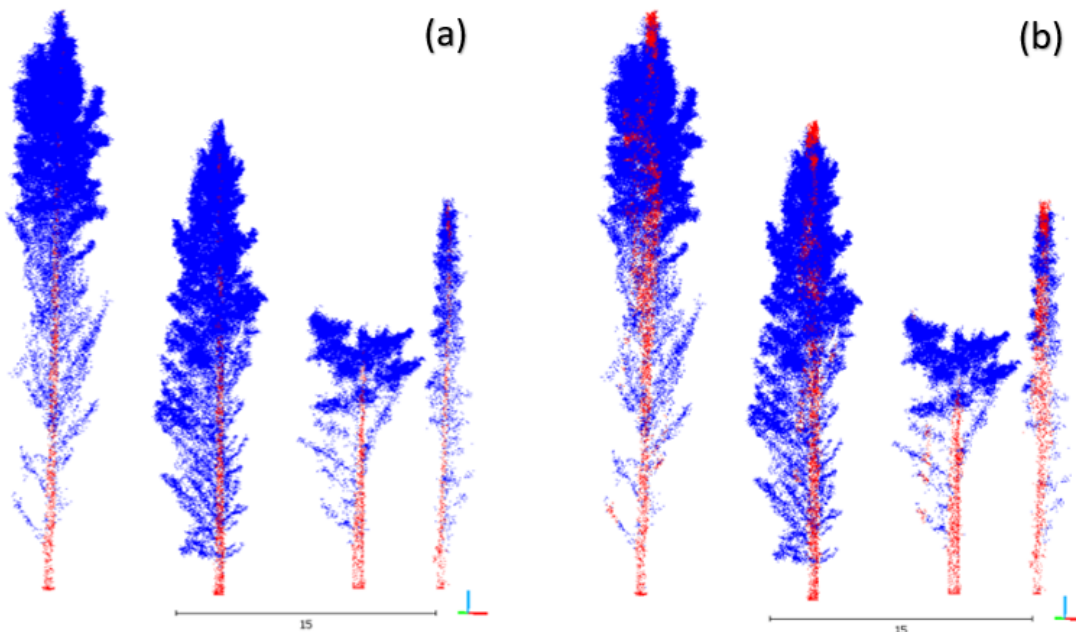


Figure 8. Figure showing profile view of 4 of the study trees with stems segmented in red manually (a) and by Voxel 3D-FCN model (b).

The results of the tree segmentation algorithm (Table 3) showed a high level of recall for stem identification (0.91) and branch and foliar identification (0.85). There was a high level of precision for branch and foliar point identification (0.99); however, precision for stem classification was relatively low (0.27). The IoU for the point classification of foliage and branching was also high at 0.84, with

IoU for stem point classification again performing relatively poorly at 0.26. Figure 8 shows a comparison of four of the trees segmented in the test data set.

4.2. DIAMETER AT BREAST HEIGHT

Comparison of predicted diameter at breast height (DBH) from the Hovermap with field measured DBH returned a strong correlation of $R^2 = 0.9$ (Figure 9f). The precision of the Hovermap measurements was relatively high with RMSE of 3.42 cm/9.95%, and an MBE of ~0 cm.

4.3. TREE HEIGHT PREDICTION

The results for both MiniVUX and Hovermap data both showed a relatively weak correlation with field-measured heights ($R^2 = 0.24$ and 0.22 respectively) (Figure 9a and 9c). The RMSE was high for both scanners at ~28.6% with a mean bias error of -3.57 m for the MiniVUX and -3.46 m for the Hovermap

(Table 4). Further analysis highlighted that most of the significantly over-estimated heights were for suppressed trees, or trees with broken tops. Once suppressed and broken trees (anything <20 m in height) were removed from the analyses, correlation with field measurements increased to R^2 values of 0.42 for MiniVUX and 0.41 for Hovermap (Figure 9b and 9d), and improvements to RMSE and MBE with 10.14% and -1.32 m for MiniVUX and 9.9% and -1.18 m for Hovermap (Table 4). Correlation between the MiniVUX and Hovermap sensors was very strong with an R^2 value of 0.94 (Figure 9e), an RMSE of 3.02% and an MBE of 0.11 m (Table 4).

Table 4. Table showing the precision and bias for comparisons between point cloud-derived height estimations and field measured heights.

Variables	R²	RMSE (m)	RMSE (%)	MBE (m)
MiniVUX vs Field	0.24	7.19	28.60	-3.57
MiniVUX vs Field (minus suppressed)	0.42	2.85	10.14	-1.32
Hovermap vs Field	0.22	7.19	28.57	-3.46
Hovermap vs Field (minus suppressed)	0.41	2.78	9.90	-1.18
MiniVUX vs Hovermap	0.94	0.87	3.02	0.11

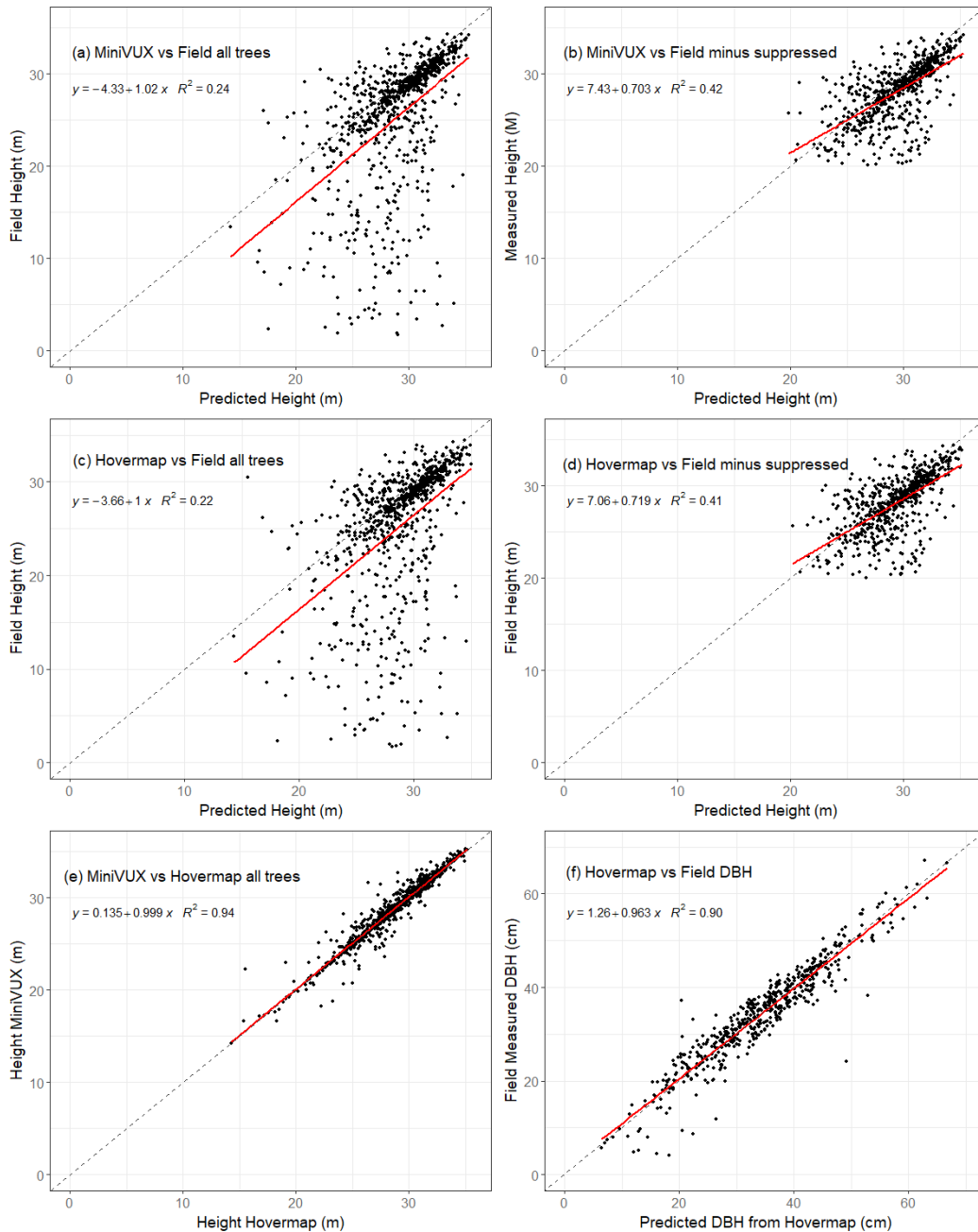


Figure 9. Correlation between field measurements and predicted height from MiniVUX data with (a) and without (b) suppressed trees, and from Hovermap map data with (c) and without (d) suppressed trees. Plot (e) shows correlation between MiniVUX and Hovermap heights. Plot (f) shows correlation between field measured and Hovermap predicted DBH. Dashed lines represent 1:1 line and red lines represent a fitted linear model with linear equation and R^2 shown.

Table 5. Tree-level results of the volumetric calculations and whorl detection from Hovermap data. Results include the maximum height of stem included in the volume calculations by the algorithm, calculated stem volume, and the height of the highest whorl predictions for 5 cm, 10 cm and 20 cm configurations, with the mean heights.

	Individual Tree Identifier												
	A8	B23	C7	D14	E8	F19	G18	H7	J5	K1	L8	M7	Mean
Max Ht (m)	13.9	14.0	10.5	10.1	17.9	10.8	12.9	9.1	17.1	15.8	18.9	17.9	14.07
Stem volume (m ³)	2.77	1.59	0.99	0.97	2.15	1.03	1.27	0.69	2.69	3.80	3.90	2.80	NA
Max Ht Whorl (5 cm)	15.38	16.0	13.1	16.3	17.6	16.6	16.7	14.7	13.7	15.4	18.4	17.4	15.99
Max Ht Whorl (10 cm)	16.1	16.9	15.4	18.1	17.5	18.8	18.1	13.5	17.1	15.9	18.6	17.6	16.97
Max Ht Whorl (20 cm)	16.15	17.1	15.1	19.1	18.7	18.9	18.7	15.1	17.1	16.3	18.5	19.3	17.55

4.4. STEM VOLUME

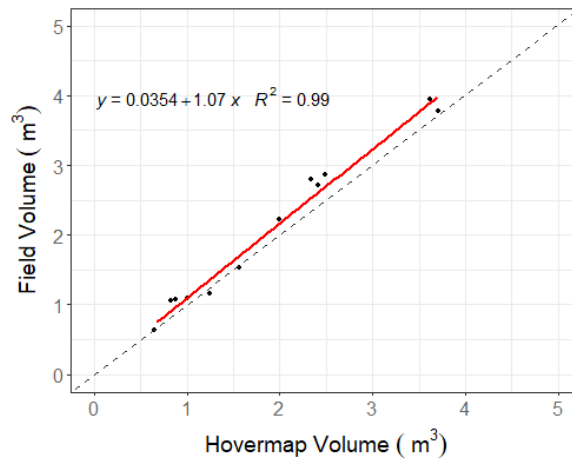


Figure 10. Correlation between field measurements for volume with volumes predicted from Hovermap data. Dashed line represents 1:1 line and red line represents a fitted linear model with linear equation and R^2 shown.

Stem volume estimates from the Hovermap data showed a very strong correlation with field-measured volumes with an R^2 value of 0.99 (Figure 10). Results had an RMSE of 0.21 m³ or 10.16%, with a mean bias error of 0.16 m³. Cylinder-fitting failures occurred at various heights for the trees assessed (Table 5). Consequently, stem volume is directly linked to the height up to which the algorithm was able to calculate volume.

4.5. WHORL DETECTION

Analysis of whorl detection was measured in two ways. First, the accuracy of whorl height measurements as predicted by the algorithm was assessed via a linear regression (Figure 11). This involved assessment of true positive whorl predictions only. Second, the ability of the algorithm to correctly identify whorls on each tree stem was assessed. The algorithm assesses stem diameters, averaged over a specified stem length, with neighbouring stem diameters. For assessment, the algorithm was tuned with 5 cm, 10 cm and 20 cm stem lengths.

All three settings for the algorithm returned a very high strong correlation for whorl height prediction ($R^2 = \sim 1.0$), with an equally high level of precision (RMSE % ranging from 17 cm/1.88% to 26 cm 2.73%) and a low level of bias, with all algorithms showing an MBE of ~ 1 cm (Table 6). The detection accuracy was, however, only moderate, ranging from 40.25% for the 5 cm tuning, and 42.41% for the 10 cm tuning (Table 6). The 20 cm configuration was able to characterise branches higher up the stem to a mean height of 17.55 m and a maximum of 19.35 m, compared to a mean of 16.97 m and maximum of 18.8 m for the 10 cm configuration, and 15.99 m and 18.48 m for the 5 cm configuration (Table 6).

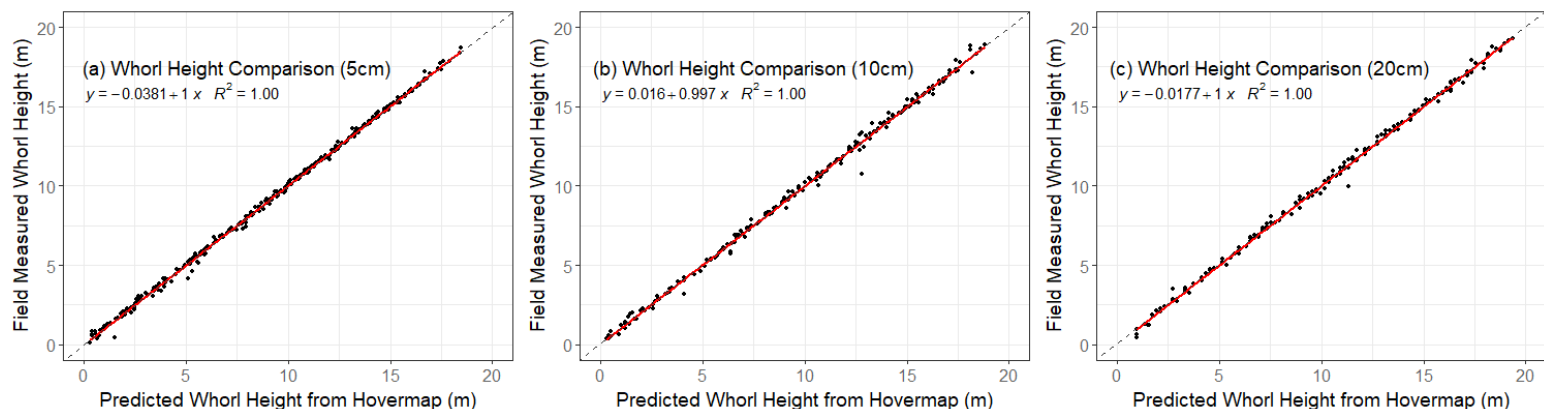


Figure 11. Correlation between field measured whorl heights with predicted whorl heights from the Hovermap data with whorl detection algorithm configured to stem segments of 5 cm (a), 10 cm (b) and 20 cm (c). Dashed lines represent 1:1 line and red lines represent a fitted linear model with linear equation and R^2 shown.

Table 6. Results for whorl detection accuracy along with values for precision and bias for each of the three configurations of the detection algorithm.

Tuning (cm)	No. whorls measured	No. Whorls detected	No. True Positives	No. False Positives	No. False negatives	R ²	RMSE (m)	RMSE (%)	MBE (m)	Detection Accuracy (%)
5	410	602	289	313	108	0.999	0.17	1.88	-0.01	40.25
10	410	265	201	64	209	0.997	0.26	2.73	-0.01	42.41
20	410	193	175	18	235	0.998	0.22	2.10	-0.01	40.89

5. DISCUSSION

In this study, a comprehensive data set was successfully captured, combining ultra-high density lidar point clouds, from both above and below the forest canopy, with field measurements. Additionally, the CloudReg methodology developed within this study enabled the accurate combination of all three streams of data at the individual tree level, which to the best of our knowledge has not been done at this scale before. Ancillary field measurements from crown mapping allowed for more intense scrutiny of metrics derived from the below-canopy laser scanning and give us greater confidence in the abilities of this technology. The results of our study overall were very promising for these novel, high-density laser scanning technologies. Methods for the extraction of a variety of phenotypic metrics were assessed and will be discussed below.

5.1. TREE STEM SEGMENTATION USING DEEP LEARNING

As a part of this study, one of our objectives was to assess the applicability of deep learning (DL) algorithms to single tree phenotyping.

The ULS data captured as a part of this study, was captured in partnership with data utilised in another project (Puliti, et al., 2021). Using MiniVUX data only, this project took 135 trees from the data set and manually annotated them into their individual component parts: stem points and branch plus foliage points. Due to resource constraints and the large amounts of annotated data required to train DL models, it was decided to utilise this resource as training data for the study. Future study should be focused on application of these DL methodologies to Hovermap data to see how they compare.

The results for the MiniVUX data set showed high recall for stem points, and low IoU and precision. The high recall score for the stem class means that most stem points manually identified in the point cloud were correctly predicted by the model. Precision and IoU scores were relatively low for stem, but high for foliage. This means that many foliage points were incorrectly segmented into the stem category. There are two likely key reasons for this (i) the up-sampling of the voxelised model predictions introduces errors as foliage points near the stem are assigned to the stem class and (ii) the model was not able to properly learn what a stem looks like, likely due to the small training data set available (117 trees). For example, a few stems in the training data set had heavy leaning and forking which can be confusing for a model when these situations are underrepresented in the training examples. Despite low precision and IoU for the stem class, with the high recall score we would expect that robust stem reconstruction algorithms will be able to fit coherent stem models to the derived stem point clouds. In the same manner as circles are fitted to stem points, the mis-segmented foliage points will be ignored as outliers, likely yielding good estimates of stem diameter from ULS in the future. Future investigations should focus on training these algorithms with much larger data sets, including additional variables in the model e.g. backscatter intensity values, and applying stem-reconstruction algorithms to the outputs to assess whether ULS data is suitable for deriving metrics such as DBH and stem volume.

Our results were compared with Windrim, et al. (2020) who used the same methodology tested on 31 (26 year old) and 39 (23 year old) *P. radiata* trees in plantation forests in NSW, Australia. Point cloud density was approximately 300-700 points per square metre. Windrim, et al. (2020) also report

relatively high scores for all metrics for foliage, and lower scores for stem. Their performance scores were generally better (e.g. foliage recall of 0.97-0.98 compared with 0.85 for this study), particularly for IoU and precision for the stem class; however, there was still room for improvement of stem detections. Differences in results may be due several factors such as (i) the appearance, variation and complexity of the trees – some of ours were leaning and forking; (ii) data capture parameters/point density; (iii) possible differences in manual annotation techniques (iv) size of training data sets – ours was twice as large, and (v) the way the training, validation, and testing sets were chosen.

Their results suggest a better trade-off between precision and recall for the stem category, with recall values of 0.64-0.77 (compared to 0.91 in this study), and precision values of 0.51-0.60 (compared with 0.27). However, it could be argued that this is an undesirable trade-off as lower recall values mean that proportionately more stem points were mis-classified by the model compared to this study. This is likely to have negative flow on effects for post segmentation analysis, e.g. computing DBH via stem reconstruction when stem points are already sparse in the raw data.

5.2. DIAMETER AT BREAST HEIGHT

Attempts were made to derive DBH measurements from the MiniVUX data. Despite the substantial pulse density, there were still not enough stem returns to fit circles and derive a measurement. This finding is supported by a previous study using the MiniVUX in a lower-stocked stand of radiata that could not obtain sufficient stem points to derive any metrics other than height (Dash, et al., 2019). Other studies have had more success in characterising stem points using the MiniVUX in other forest types (Bruggisser, et al., 2020) which could suggest that species has a greater influence over the number stem returns. Future study should be focused on assessing this technology in different forest environments.

Only 544 stems (61.5%) of the trees in this study were able to be segmented using the SimpleForest pipeline. We speculate that reasons for this could involve the inclusion of 79 trees that had a DBH of <10cm. The rigorous filtering required to derive stems from the larger trees could have removed a lot of these smaller diameter trees, which have previously been noted as difficult to measure with MLS (Ryding, et al., 2015). The stand also was planted in a 1.5 m x 5 m spacing and was never thinned, resulting in areas of high stem density, which caused some issues for the algorithm. Future study to refine the methods for stem delineation and particularly utilising DL methods is encouraged.

Results of this study showed a high level of correlation between field and Hovermap measurements for DBH ($R^2 = 0.90$). Compared to the literature, our results fall short of the reported correlations of $R^2 = 0.99$ for other SLAM-based MLS studies (Bauwens, et al., 2016; Giannetti, et al., 2018) and studies focused on TLS, with an R^2 range of 0.93-0.99 (Bauwens, et al., 2016; Calders, et al., 2015; Chen, et al., 2019; Giannetti, et al., 2018). The precision of the DBH measurements (RMSE = 3.42 cm/9.95%) was also towards the lower end of results reported in the literature for TLS studies (RMSE = 1.13-3.37cm/5.4-13.4%) (Bauwens, et al., 2016; Calders, et al., 2015; Čerňava, et al., 2017; Chen, et al., 2019; Giannetti, et al., 2018; Hyypä, et al., 2020) and for SLAM-based MLS studies (1.11-2.9 cm/3.4-23%) (Bauwens, et al., 2016; Giannetti, et al., 2018; Hyypä, et al., 2020; Ryding, et al., 2015).

Tuning of the variable height DBH algorithm developed in this study could be one reason for the lower levels of correlation and precision. In accordance with field measurement practice in NZ (CNI Regional YTGEM User Group, 2007), DBH was measured within 10 cm of 1.4 m above the ground. If there was swelling, DBH was calculated from measurements were taken from two internodal sections at equal distances above and below the swollen 1.4 mark in what is termed a “split”. When removing the split measurements from the data set, improvements to the RMSE of 0.08cm/0.18% were observed. Another reason could be due to the accuracy of field measurements. Although the utmost care was taken to ensure the accuracy of measurements, human error cannot be discounted from the field measurements and some obvious errors were noted and removed. To avoid this scenario, other studies have compared MLS data with TLS data (Bauwens, et al., 2016; Cabo, Del Pozo, et al., 2018; Ryding, et al., 2015).

5.3. HEIGHT

Levels of precision and correlation between both the Hovermap ($R^2 = 0.22$ / RMSE = 7.19 m /28.57%) and the MiniVUX ($R^2 = 0.24$ / RMSE of 7.9 m/28.6%) with field data were relatively low. When compared to the literature, this is unusually weak with previous studies on TLS reporting an RMSE of between 0.54 m and 6 m (Cabo, Ordóñez, et al., 2018; Fleck, et al., 2011; Huang, et al., 2011; Liang, et al., 2013; Maas, et al., 2008; Moskal, et al., 2012) and R^2 values ranging from 0.57 to 0.95 (Fleck, et al., 2011; Huang, et al., 2011; Moskal, et al., 2012). Results in the literature for ULS also show a much higher level of correlation with R^2 values ranging from 0.76 to 0.97 (Camarretta, et al., 2020; Corte, et al., 2020; Jaakkola, et al., 2017; Puliti, et al., 2020; Sankey, et al., 2017) and precision with RMSE 0.72% to 7.91% (Corte, et al., 2020; Hyyppä, et al., 2020; Jaakkola, et al., 2017; Liang, et al., 2019; Puliti, et al., 2020). These poor results can largely be attributed to the over-estimation of height for suppressed trees within the stand. Figure 12 shows an example of two suppressed trees which were overestimated by ~15 m by both scanners.

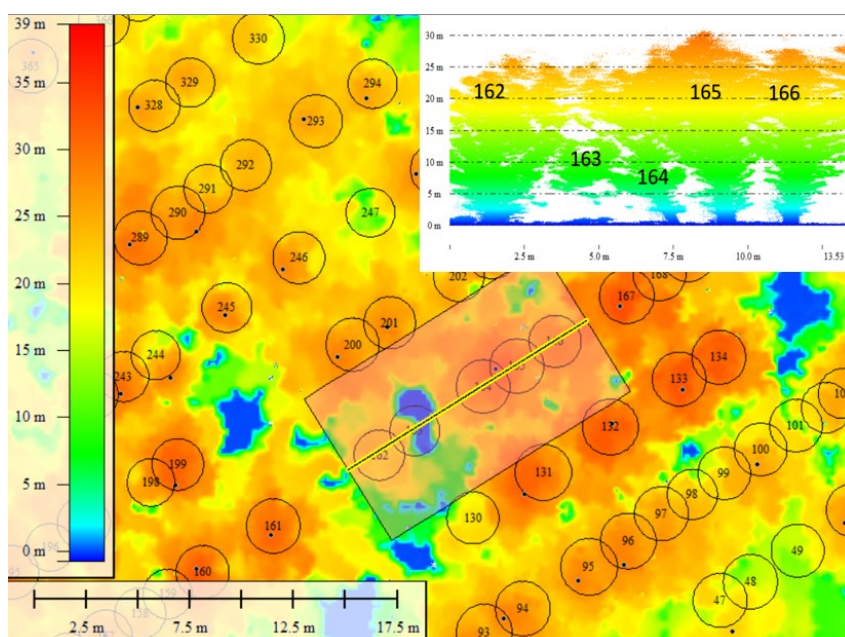


Figure 12. Nadir view of two suppressed tree in the CHM, and inset as a transect, highlighting the issue of using peak-detection for suppressed trees.

When the suppressed and broken trees were removed from the results of this study, significant improvements in agreement ($R^2 = 0.42$ and 0.41) and precision (RMSE 2.85 m/10.14% and 2.78 m/9.9%) were observed for the MiniVUX and Hovermap scanners respectively. This is consistent with findings of a previous study, which found a much higher level of precision with unbroken trees (RMSE 6.8%) compared with broken trees (RMSE = 56%), the inclusion of which significantly affected overall precision (RMSE = 15%) (Dash, et al., 2019).

The negative effect of suppressed trees on the results implies that the peak detection methodology is not appropriate for single tree-level height measurement in mature stands. This is a common finding in the literature, and alternate methods for tree height detection have been proposed to compensate for this (Ayrey, et al., 2017). Future studies should look to apply these algorithms to MLS and ULS at an individual tree level to assess their efficacy.

The potential impact of the time lag between data captures must also be considered. Comparisons with a prior MiniVUX data capture of the site reveal an average 1.45 m increase in peak height from May 2020 to May 2021. Due to delays in the project cause by COVID-19, the MiniVUX and Hovermap data sets were captured 9 months and 11 months respectively after the field data.

Additionally, tree height is notoriously difficult to capture in the field and even an experienced mensuration forester can have trouble accurately attaining height due to occlusion, tree lean or intertwined tree tops (Wang, et al., 2019). To remove this potential source of error, the field heights were

replaced with MiniVUX heights based on findings from a previous study showing that the MiniVUX is capable of measuring tree heights with a high level of precision and accuracy ($R^2 = 0.99$, $RMSE = 5.91\%$) (Hartley, et al., 2020). The results were extremely encouraging, demonstrating a strong correlation ($R^2 = 0.94$) and a low level of error, with an $RMSE$ of 0.87 m. Interestingly, the MBE of 11 cm between the two scanners indicated that the estimates from the Hovermap were slightly higher than the MiniVUX. This would also suggest that the Hovermap may be capable of more accurate measurements of mature trees from the ground than the MiniVUX can obtain from the air, as previous studies have found the MiniVUX to have a slight negative bias ($MBE = 0.05\text{m}$) (Hartley, et al., 2020). This is a significant finding, as previous research has indicated that TLS and MLS are both prone to underprediction of tree height due to the low range of the scanners, and the occlusion caused by branching (Cabo, Del Pozo, et al., 2018).

5.4. STEM VOLUME

Results from stem volume assessments found that the Hovermap estimates were very strongly correlated with field measurements ($R^2 = 0.99$). Estimates demonstrated a moderately high level of precision ($RMSE = 0.21 \text{ m}^3/10.16\%$) and a tendency to underestimate volumes ($MBE = 0.16 \text{ m}^3$). These findings fit well with existing studies that have shown underestimation of between 6.8% and 15% of total stem volume (Dassot, et al., 2012; Hyyppä, et al., 2020; Murphy, 2008; Saarinen, et al., 2017). Of these studies, the closest methodology to that used in this study reported a general underestimation of stem volume of up to 10% when comparing TLS to destructive sampling methods (Dassot, et al., 2012).

There was a slight inversely proportionate decrease in accuracy with an increase of total stem volume (Figure 10). As expected, the volume per tree is firmly related to the height up the stem up to which the algorithm was able to derive volume (Table 5). One possible reason for this increase in volumetric error could be associated with an increase in the diametric error of the point cloud higher up the stem. This would manifest itself as greater error in tree volumes that include a greater proportion of stem length. This is not an uncommon phenomenon, and has been observed in other studies using TLS and ULS (Brede, et al., 2019; Bruggisser, et al., 2020; Maas, et al., 2008; Wang, et al., 2016).

On average, the volumetric algorithms deployed in this study were able to calculate volumes up to ~14 m, with a minimum and maximum height of 9.1 m and 18.9 m. In their study, Bruggisser, et al. (2020), calculated that 71.9% of total stem volume could be found within the first 10 m of the stem. Using this logic, measurements from the Hovermap should be able to account for a minimum of two thirds of the tree's volume with an accuracy of ~90%. Future research should be focused on better understanding the interaction between stem curve and diametric error for the Hovermap. A better understanding of this relationship, along with the development of methods to derive volume from areas of the stem point cloud with lower pulse density, could aid in the development of usable models for deriving stem volume from Hovermap point clouds.

5.5. WHORL DETECTION

All three configurations of the whorl detection algorithm showed high levels of precision (Figure 11) and correlation (Table 6) with field measurements for whorl height when manually aligned. The whorl detection algorithm also outperformed the volume calculation algorithm in terms of proportion of the stem covered (Table 6), with the best configuration (20 cm) detecting whorls up to a max height of 19.35 m and a mean height of 17.55 m. This is likely because the cylinder fitting algorithm struggled to fit cylinders to sections of the stem higher up the tree (see Figure 7).

The whorl detection accuracy was somewhat lower than the whorl height accuracy. The highest and lowest accuracy was achieved by the 10 cm (42.41%) and 5 cm (40.25%) configurations, with false positive rates of ~24% and ~52% respectively. The 5 cm configuration was able to correctly identify the most whorls (~70%); however, it also generated nearly fivefold more false positives than the best configuration. Similar work by Pyörälä, et al. (2018) used clusters of detected branches to identify whorl locations on the stem. Their algorithm correctly detected only slightly more whorls than the

algorithm in this study, at 71.1%; however, the low number of false positives (1.9%) increased the overall detection accuracy to 69.9% (compared with 40-42% in this study). This is approximately thirteen times less false positives than the best results of this study. Possible reasons for this large difference in detection could be due to their use of TLS, which is known to create less noisy point clouds than the MLS system used in this study (Tang, et al., 2015). Their reported mean lowest whorl height was also above 7 m high, with a maximum lowest whorl height of 13.5 m, due to self-pruning of the studies species. This would indicate that the stems had fewer branches than the radiata in our study which were pruned up to ~2 m. This would generate more noise in the Hovermap point clouds. The whorl detection method also focused on branch detection and conglomeration, rather than identification of stem swelling. Future study should be focused on methods for reducing the number of false positives identified, possibly by integrating branch and stem swelling detection to improve overall accuracy.

6. CONCLUSIONS

This study has shown that accurate phenotypic measurements can be derived from mature stands of *P. radiata* using Mobile Laser Scanning (MLS) units, such as the Hovermap. From MLS point clouds, a range of measurements, including stem volume and diameter at breast height (DBH) can be extracted with a high level of precision and accuracy. This technology also shows very real potential for reducing field capture times when compared with traditional inventory methods. Once algorithms for deriving metrics are fine-tuned, standardised and more widely available, there is a very real potential for high-throughput phenotyping or inventory capture at scale. The Hovermap is a relatively affordable solution, when compared to a high-end scanner such as the MiniVUX and provides a range of different use configurations suited to different forest conditions and tasks.

A key finding of this study has been that, from the ground, the Hovermap is able to derive canopy heights with a level of precision and accuracy comparable to the MiniVUX from the air. This finding has significant implications for forestry as it has previously been necessary to use laser scanners both above and below the forest canopy to estimate tree height and characterise stems from the same point cloud.

Despite increasing the pulse density to an order of magnitude larger than a standard ULS capture, our findings indicate that ULS is less useful for phenotyping. We were only able to derive heights from the data, which did not perform well in a mature forest canopy. DL shows some promise for efficiency gains for the delineation of tree stems, and with more work could increase the usability of ULS through derivation of further crucial metrics such as DBH and volume.

There is more work required in fine-tuning algorithms and, in particular, methods for improved tree height extraction from point clouds captured from mature stands. Additionally, fine-tuning of the methodology for whorl detection and building on this to be able to characterise branch size should also be an area for future focus. Testing of this equipment in more diverse forest environments, with varied ages, stand densities or levels of undergrowth would also be highly beneficial. Overall, this technology holds significant potential as a means of advancing forest mensuration and phenotyping towards a digital future.

ACKNOWLEDGEMENTS

We would like to thank Liam Wright for his assistance with Hovermap data capture in the wider project. We would also like to thank Alan Tan and David Pont for their involvement in the development of this project. We would also like to acknowledge Forest and Woodlot Inventory Services for capture of the mensuration data for this study.

GLOSSARY

Above Ground Level (AGL) – Measurement of altitude used in aviation for the distance between an aircraft and the ground (as opposed to distance between the ground and mean sea level).

Autonomy Level 1 (AL1) – Term assigned to the first level of autonomous flight control in the Hovermap unit. This mode allows for the pilot to fly the craft manually but with the Hovermap acting as an industrial-grade object avoidance unit, minimising the risk of collision, and allowing for flight stabilisation without the need for GNSS (see below).

Autonomy Level 1 (AL2) – Term assigned to the second level of autonomous flight control in the Hovermap unit. This mode allows for fully autonomous flight, in which the pilot can assign a flight route to the craft utilising waypoints, and the Hovermap will act as the craft's with navigation aid, replacing GNSS, maintaining altitude and minimising the risk of collision.

Airborne Laser Scanning (ALS) – A method of aerial survey utilising lidar (see LiDAR below) to create a three-dimensional model of a real work environment, known as a point cloud (see below). This term is almost exclusively applied to the airborne collection of lidar data from a manned aircraft, as opposed to a UAV (see below), but can be used interchangeably.

Deep Learning (DL) – A method of machine learning that utilises artificial neural networks to mimic the structure and function of the human brain allowing computer algorithms to perform both feature extraction and classification.

Global Navigation Satellite System (GNSS) – A Navigation methodology relying on triangulation of position through the use of satellite constellations. Many constellations are currently operational, including GPS (US), BEIDOU (China), GLONASS (Russia) and GALILEO (EU).

Ground Control Point (GCP) – A physical marker applied to an area of interest prior to remote sensing survey that is clearly visible in the remotely sensed imagery. These points are surveyed using GNSS to give that point high accuracy, so that this information can then be utilised to enhance the spatial accuracy of the geospatial model produced.

Inertial Motion Unit (IMU) – A device that measures orientation, angle and acceleration of a machine or craft. Generally used in combination with a GNSS (see above) to locate a machine or craft in the real world and aid in navigation.

Light Detection and Ranging (LiDAR) – A remote sensing method that utilises light-based range finding to calculate distances between the scanner and its environment. Analogous with term “laser scanning”.

Mobile Laser Scanning (MLS) – A laser scanning methodology that incorporates a laser scanner with a mobile platform in order to build point clouds whilst moving. This term can apply to vehicle-mounted, backpack-mounted or handheld configurations of laser scanner.

Point Cloud – A three-dimensional model of spatial points usually collected through laser scanning or photogrammetric methodologies which represents a real-world environment or object.

Post-processed Kinematic (PPK) – A methodology for correcting GNSS (see above) data from a roving antenna to centimetre or decimetre level precision by utilising highly accurate positional data from a base antenna. This correction is applied after the data has been collected.

Pulses per square meter (ppm²) – Unit of measurement for the density of points in a point cloud.

Simultaneous Localisation and Mapping (SLAM) – A methodology for the sensing and mapping of an environment generally used in robotics or automation to enable an autonomous machine to locate

itself in a real-world environment, whilst building a map of the environment it moves through. This technique often utilises laser scanning as the primary method for sensing.

Terrestrial Laser Scanning (TLS) – Methodologies for laser scanning of environments or objects from the ground. This term is often used to refer to static, or tripod-mounted laser scanners, but can also be used as a more general term encompassing mobile laser scanners (MLS – see above).

Unmanned Aerial Vehicle (UAV) – An airborne robot that is controlled by a pilot on the ground. Predominantly used for aerial survey, but increasingly being used for multiple additional applications, including agricultural chemical application or sample collection.

UAV Laser Scanning (ULS) – A method of airborne laser scanning (see above) that utilises UAVs (see above) as the platform for carrying the scanner, rather than a manned aircraft (ALS – see above).

REFERENCES

- Abadi, M., Agarwal, A., Barham, P., Brevdo, E., Chen, Z., Citro, C., Corrado, G. S., Davis, A., Dean, J., & Devin, M. (2016). Tensorflow: Large-scale machine learning on heterogeneous distributed systems. *arXiv preprint arXiv:1603.04467*.
- Abegg, M., Kükenbrink, D., Zell, J., Schaepman, M. E., & Morsdorf, F. (2017). Terrestrial laser scanning for forest inventories-tree diameter distribution and scanner location impact on occlusion. *Forests*, 8(6). doi:10.3390/f8060184
- Ayrey, E., Fraver, S., Kershaw Jr, J. A., Kenefic, L. S., Hayes, D., Weiskittel, A. R., & Roth, B. E. (2017). Layer stacking: a novel algorithm for individual forest tree segmentation from LiDAR point clouds. *Canadian Journal of Remote Sensing*, 43(1), 16-27.
- Bauwens, S., Bartholomeus, H., Calders, K., & Lejeune, P. (2016). Forest inventory with terrestrial LiDAR: A comparison of static and hand-held mobile laser scanning. *Forests*, 7(6). doi:10.3390/f7060127
- Bentley, J. L. (1975). Multidimensional binary search trees used for associative searching. *Communications of the ACM*, 18(9), 509-517.
- Bienert, A., Georgi, L., Kunz, M., Maas, H. G., & von Oheimb, G. (2018). Comparison and combination of mobile and terrestrial laser scanning for natural forest inventories. *Forests*, 8(2). doi:10.3390/f9070395
- Bombrun, M., Dash, J. P., Pont, D., Watt, M. S., Pearse, G. D., & Dungey, H. S. (2020). Forest-Scale Phenotyping: Productivity Characterisation Through Machine Learning. *Frontiers in Plant Science*, 11(99). doi:10.3389/fpls.2020.00099
- Boudon, F., Preuksakarn, C., Ferraro, P., Diener, J., Nacry, P., Nikinmaa, E., & Godin, C. (2014). Quantitative assessment of automatic reconstructions of branching systems obtained from laser scanning. *Annals of Botany*, 114(4), 853-862. doi:10.1093/aob/mcu062
- Braga, J. R. G., Peripato, V., Dalagnol, R., Ferreira, M. P., Tarabalka, Y., Aragão, L. E. O. C., de Campos Velho, H. F., Shiguemori, E. H., & Wagner, F. H. (2020). Tree crown delineation algorithm based on a convolutional neural network. *Remote Sensing*, 12(8). doi:10.3390/RS12081288
- Brede, B., Calders, K., Lau, A., Raunonen, P., Bartholomeus, H. M., Herold, M., & Kooistra, L. (2019). Non-destructive tree volume estimation through quantitative structure modelling: Comparing UAV laser scanning with terrestrial LIDAR. *Remote Sensing of Environment*, 233. doi:10.1016/j.rse.2019.111355
- Bruggisser, M., Hollaus, M., Otepka, J., & Pfeifer, N. (2020). Influence of ULS acquisition characteristics on tree stem parameter estimation. *ISPRS Journal of Photogrammetry and Remote Sensing*, 168, 28-40. doi:10.1016/j.isprsjprs.2020.08.002
- Bu, G., & Wang, P. (2016). Adaptive circle-ellipse fitting method for estimating tree diameter based on single terrestrial laser scanning. *Journal of Applied Remote Sensing*, 10(2). doi:10.1117/1.JRS.10.026040
- Buck, A. L. B., Lingnau, C., Neto, S. P., Machado, Á. M. L., & Martins-Neto, R. P. (2019). Stem modelling of eucalyptus by terrestrial laser scanning. *Floresta e Ambiente*, 26(4). doi:10.1590/2179-8087.012516
- Cabo, C., Del Pozo, S., Rodríguez-González, P., Ordóñez, C., & González-Aguilera, D. (2018). Comparing Terrestrial Laser Scanning (TLS) and Wearable Laser Scanning (WLS) for Individual Tree Modeling at Plot Level. *Remote Sensing*, 10(4). doi:10.3390/rs10040540
- Cabo, C., Ordóñez, C., López-Sánchez, C. A., & Armesto, J. (2018). Automatic dendrometry: Tree detection, tree height and diameter estimation using terrestrial laser scanning. *International Journal of Applied Earth Observation and Geoinformation*, 69, 164-174. doi:10.1016/j.jag.2018.01.011
- Calders, K., Newnham, G., Burt, A., Murphy, S., Raunonen, P., Herold, M., Culvenor, D., Avitabile, V., Disney, M., Armston, J., & Kaasalainen, M. (2015). Nondestructive estimates of above-ground biomass using terrestrial laser scanning. *Methods in Ecology and Evolution*, 6(2), 198-208. doi:10.1111/2041-210X.12301
- Camarretta, N., Harrison, P. A., Lucieer, A., Potts, B. M., Davidson, N., & Hunt, M. (2020). From drones to phenotype: Using UAV-LiDAR to detect species and provenance variation in tree productivity and structure. *Remote Sensing*, 12(19), 1-16. doi:10.3390/rs12193184

- Čerňava, J., Tuček, J., Koreň, M., & Mokroš, M. (2017). Estimation of diameter at breast height from mobile laser scanning data collected under a heavy forest canopy. *Journal of Forest Science*, 63(9), 433-441. doi:10.17221/28/2017-JFS
- Chen, S., Feng, Z., Chen, P., Khan, T. U., & Lian, Y. (2019). Nondestructive estimation of the above-ground biomass of multiple tree species in boreal forests of china using terrestrial laser scanning. *Forests*, 10(11). doi:10.3390/f10110936
- CNI Regional YTCEN User Group, N. (2007). PlotSafe: OVERLAPPING FEATURE CRUISING. Forest Inventory Procedures.
- Corte, A. P. D., Rex, F. E., de Almeida, D. R. A., Sanquetta, C. R., Silva, C. A., Moura, M. M., Wilkinson, B., Zambrano, A. M. A., da Cunha Neto, E. M., Veras, H. F. P., de Moraes, A., Klauberg, C., Mohan, M., Cardil, A., & Broadbent, E. N. (2020). Measuring individual tree diameter and height using gatereye high-density UAV-lidar in an integrated crop-livestock-forest system. *Remote Sensing*, 12(5). doi:10.3390/rs12050863
- Costa, C., Schurr, U., Loreto, F., Menesatti, P., & Carpentier, S. (2018). Plant Phenotyping Research Trends, a Science Mapping Approach. *Front Plant Sci*, 9, 1933. doi:10.3389/fpls.2018.01933
- Dash, J. P., Watt, M. S., & Hartley, R. J. L. (2019). Testing UAV-borne Riegl Mini VUX-1 scanner for phenotyping a mature genetics trial.
- Dassot, M., Colin, A., Santenoise, P., Fournier, M., & Constant, T. (2012). Terrestrial laser scanning for measuring the solid wood volume, including branches, of adult standing trees in the forest environment. *Computers and Electronics in Agriculture*, 89, 86-93.
- de Conto, T., Olofsson, K., Görgens, E. B., Rodriguez, L. C. E., & Almeida, G. (2017). Performance of stem denoising and stem modelling algorithms on single tree point clouds from terrestrial laser scanning. *Computers and Electronics in Agriculture*, 143, 165-176.
- Dungey, H. S., Dash, J. P., Pont, D., Clinton, P. W., Watt, M. S., & Telfer, E. J. (2018). Phenotyping Whole Forests Will Help to Track Genetic Performance. *Trends Plant Sci*, 23(10), 854-864. doi:10.1016/j.tplants.2018.08.005
- Fleck, S., Mölder, I., Jacob, M., Gebauer, T., Jungkunst, H. F., & Leuschner, C. (2011). Comparison of conventional eight-point crown projections with LIDAR-based virtual crown projections in a temperate old-growth forest. *Annals of forest science*, 68(7), 1173-1185.
- Giannetti, F., Puletti, N., Quatrini, V., Travaglini, D., Bottalico, F., Corona, P., & Chirici, G. (2018). Integrating terrestrial and airborne laser scanning for the assessment of single-tree attributes in Mediterranean forest stands. *European Journal of Remote Sensing*, 51(1), 795-807. doi:10.1080/22797254.2018.1482733
- Hackenberg, J., Calders, K., Demol, M., Raunonen, P., Piboule, A., & Disney, M. (2021). SimpleForest-a comprehensive tool for 3d reconstruction of trees from forest plot point clouds. *bioRxiv*.
- Hartley, R. J., Leonardo, E. M., Massam, P., Watt, M. S., Estarija, H. J., Wright, L., Melia, N., & Pearse, G. D. (2020). An Assessment of High-Density UAV Point Clouds for the Measurement of Young Forestry Trials. *Remote Sensing*, 12(24), 4039.
- Holopainen, M., Kankare, V., Vastaranta, M., Liang, X., Lin, Y., Vaaja, M., Yu, X., Hyypä, J., Hyypä, H., & Kaartinen, H. (2013). Tree mapping using airborne, terrestrial and mobile laser scanning—A case study in a heterogeneous urban forest. *Urban forestry & urban greening*, 12(4), 546-553.
- Hopkinson, C., Chasmer, L., Young-Pow, C., & Treitz, P. (2004). Assessing forest metrics with a ground-based scanning lidar. *Canadian Journal of Forest Research*, 34(3), 573-583.
- Huang, H., Li, Z., Gong, P., Cheng, X., Clinton, N., Cao, C., Ni, W., & Wang, L. (2011). Automated methods for measuring DBH and tree heights with a commercial scanning lidar. *Photogrammetric Engineering & Remote Sensing*, 77(3), 219-227.
- Hyypä, E., Yu, X., Kaartinen, H., Hakala, T., Kukko, A., Vastaranta, M., & Hyypä, J. (2020). Comparison of backpack, handheld, under-canopy UAV, and above-canopy UAV laser scanning for field reference data collection in boreal forests. *Remote Sensing*, 12(20), 1-31. doi:10.3390/rs12203327
- Isenburg, M. (2019). LAStools - Efficient LiDAR Processing Software (Version 190404).
- Jaakkola, A., Hyypä, J., Yu, X., Kukko, A., Kaartinen, H., Liang, X., Hyypä, H., & Wang, Y. (2017). Autonomous collection of forest field reference—The outlook and a first step with UAV laser scanning. *Remote Sensing*, 9(8). doi:10.3390/rs9080785

- Kankare, V., Joensuu, M., Vauhkonen, J., Holopainen, M., Tanhuanpää, T., Vastaranta, M., Hyyppä, J., Hyyppä, H., Alho, P., Rikala, J., & Sipi, M. (2014). Estimation of the timber quality of scots pine with terrestrial laser scanning. *Forests*, *5*(8), 1879-1895. doi:10.3390/f5081879
- Kellner, J. R., Armston, J., Birrer, M., Cushman, K., Duncanson, L., Eck, C., Falleger, C., Imbach, B., Král, K., & Krůček, M. (2019). New opportunities for forest remote sensing through ultra-high-density drone lidar. *Surveys in geophysics*, *40*(4), 959-977.
- Liang, X., & Hyyppä, J. (2013). Automatic stem mapping by merging several terrestrial laser scans at the feature and decision levels. *Sensors (Switzerland)*, *13*(2), 1614-1634. doi:10.3390/s130201614
- Liang, X., Hyyppä, J., Kaartinen, H., Lehtomäki, M., Pyörälä, J., Pfeifer, N., Holopainen, M., Brolly, G., Francesco, P., Hackenberg, J., Huang, H., Jo, H. W., Katoh, M., Liu, L., Mokroš, M., Morel, J., Olofsson, K., Poveda-Lopez, J., Trochta, J., Wang, D., Wang, J., Xi, Z., Yang, B., Zheng, G., Kankare, V., Luoma, V., Yu, X., Chen, L., Vastaranta, M., Saarinen, N., & Wang, Y. (2018). International benchmarking of terrestrial laser scanning approaches for forest inventories. *ISPRS Journal of Photogrammetry and Remote Sensing*, *144*, 137-179. doi:10.1016/j.isprsjprs.2018.06.021
- Liang, X., Kankare, V., Hyyppä, J., Wang, Y., Kukko, A., Haggrén, H., Yu, X., Kaartinen, H., Jaakkola, A., Guan, F., Holopainen, M., & Vastaranta, M. (2016). Terrestrial laser scanning in forest inventories. *ISPRS Journal of Photogrammetry and Remote Sensing*, *115*, 63-77. doi:10.1016/j.isprsjprs.2016.01.006
- Liang, X., Wang, Y., Pyörälä, J., Lehtomäki, M., Yu, X., Kaartinen, H., Kukko, A., Honkavaara, E., Issaoui, A. E. I., Nevalainen, O., Vaaja, M., Virtanen, J. P., Katoh, M., & Deng, S. (2019). Forest in situ observations using unmanned aerial vehicle as an alternative of terrestrial measurements. *Forest Ecosystems*, *6*(1). doi:10.1186/s40663-019-0173-3
- Lovell, J., Jupp, D. L., Culvenor, D., & Coops, N. (2003). Using airborne and ground-based ranging lidar to measure canopy structure in Australian forests. *Canadian Journal of Remote Sensing*, *29*(5), 607-622.
- Maas, H. G., Bienert, A., Scheller, S., & Keane, E. (2008). Automatic forest inventory parameter determination from terrestrial laser scanner data. *International journal of remote sensing*, *29*(5), 1579-1593.
- Maturana, D., & Scherer, S. (2015). Voxnet: A 3d convolutional neural network for real-time object recognition. In *2015 IEEE/RSJ International Conference on Intelligent Robots and Systems (IROS)* (pp. 922-928) IEEE.
- Mengesha, T., Hawkins, M., Tarleton, M., & Nieuwenhuis, M. (2015). Stem quality assessment using terrestrial laser scanning technology: a case study of ash trees with a range of defects in two stands in Ireland. *Scandinavian Journal of Forest Research*, *30*(7), 605-616. doi:10.1080/02827581.2015.1043340
- Milletari, F., Navab, N., & Ahmadi, S.-A. (2016). V-net: Fully convolutional neural networks for volumetric medical image segmentation. In *2016 fourth international conference on 3D vision (3DV)* (pp. 565-571) IEEE.
- Moskal, L. M., & Zheng, G. (2012). Retrieving forest inventory variables with terrestrial laser scanning (TLS) in urban heterogeneous forest. *Remote Sensing*, *4*(1), 1-20.
- Murphy, G. (2008). Determining stand value and log product yields using terrestrial lidar and optimal bucking: a case study. *Journal of Forestry*, *106*(6), 317-324.
- Newnham, G. J., Armston, J. D., Calders, K., Disney, M. I., Lovell, J. L., Schaaf, C. B., Strahler, A. H., & Danson, F. M. (2015). Terrestrial Laser Scanning for Plot-Scale Forest Measurement. *Current Forestry Reports*, *1*(4), 239-251. doi:10.1007/s40725-015-0025-5
- Pearse, G. D., Watt, M. S., Dash, J. P., Stone, C., & Caccamo, G. (2019). Comparison of models describing forest inventory attributes using standard and voxel-based lidar predictors across a range of pulse densities. *International Journal of Applied Earth Observation and Geoinformation*, *78*, 341-351. doi:10.1016/j.jag.2018.10.008
- Pont, D. (2016). Assessment of individual trees using aerial laser scanning in New Zealand radiata pine forests.
- Pont, D., Dungey, H. S., Suontama, M., & Stovold, G. T. (2020). Spatial Models With Inter-Tree Competition From Airborne Laser Scanning Improve Estimates of Genetic Variance. *Front Plant Sci*, *11*, 596315. doi:10.3389/fpls.2020.596315

- Puliti, S., Dash, J. P., Watt, M. S., Breidenbach, J., & Pearse, G. D. (2020). A comparison of UAV laser scanning, photogrammetry and airborne laser scanning for precision inventory of small-forest properties. *Forestry*, 93(1), 150-162. doi:10.1093/forestry/cpz057
- Puliti, S., Pearse, G. D., Watt, M. S., Mitchard, E., McNicol, I., Bremer, M., Rutzinger, M., Surovy, P., Wallace, L., & Hollaus, M. (2021). A New Drone Laser Scanning Benchmark Dataset for Characterization of Single-Tree and Forest Biophysical Properties. In *2021 IEEE International Geoscience and Remote Sensing Symposium IGARSS* (pp. 728-730) IEEE.
- Pyörälä, J., Liang, X., Vastaranta, M., Saarinen, N., Kankare, V., Wang, Y., Holopainen, M., & Hyyppä, J. (2018). Quantitative assessment of Scots pine (*Pinus sylvestris* L.) whorl structure in a forest environment using terrestrial laser scanning. *IEEE Journal of Selected Topics in Applied Earth Observations and Remote Sensing*, 11(10), 3598-3607.
- R Core Team. (2020). R: A language and environment for statistical computing.: R Foundation for Statistical Computing, Vienna, Austria.
- Raumonen, P., Åkerblom, M., Kaasalainen, M., Casella, E., Calders, K., & Murphy, S. (2015). Massive-scale tree modelling from TLS data. *ISPRS Annals of Photogrammetry, Remote Sensing & Spatial Information Sciences*, 2.
- Roussel, J.-R., Auty, D., De Boissieu, F., & Meador, A. (2018). lidR: Airborne LiDAR data manipulation and visualization for forestry applications. *R package version*, 1(1).
- Ryding, J., Williams, E., Smith, M. J., & Eichhorn, M. P. (2015). Assessing handheld mobile laser scanners for forest surveys. *Remote Sensing*, 7(1), 1095-1111. doi:10.3390/rs70101095
- Saarinen, N., Kankare, V., Vastaranta, M., Luoma, V., Pyörälä, J., Tanhuanpää, T., Liang, X., Kaartinen, H., Kukko, A., & Jaakkola, A. (2017). Feasibility of Terrestrial laser scanning for collecting stem volume information from single trees. *ISPRS Journal of Photogrammetry and Remote Sensing*, 123, 140-158.
- Sankey, T., Donager, J., McVay, J., & Sankey, J. B. (2017). UAV lidar and hyperspectral fusion for forest monitoring in the southwestern USA. *Remote Sensing of Environment*, 195, 30-43. doi:10.1016/j.rse.2017.04.007
- Shao, J., Zhang, W., Mellado, N., Wang, N., Jin, S., Cai, S., Luo, L., Lejemble, T., & Yan, G. (2020). SLAM-aided forest plot mapping combining terrestrial and mobile laser scanning. *ISPRS Journal of Photogrammetry and Remote Sensing*, 163, 214-230. doi:10.1016/j.isprsjprs.2020.03.008
- Tang, J., Chen, Y., Kukko, A., Kaartinen, H., Jaakkola, A., Khoramshahi, E., Hakala, T., Hyyppä, J., Holopainen, M., & Hyyppä, H. (2015). SLAM-aided stem mapping for forest inventory with small-footprint mobile LiDAR. *Forests*, 6(12), 4588-4606. doi:10.3390/f6124390
- Thies, M., Pfeifer, N., Winterhalder, D., & Gorte, B. G. (2004). Three-dimensional reconstruction of stems for assessment of taper, sweep and lean based on laser scanning of standing trees. *Scandinavian Journal of Forest Research*, 19(6), 571-581.
- Torresan, C., Carotenuto, F., Chiavetta, U., Miglietta, F., Zaldei, A., & Gioli, B. (2020). Individual tree crown segmentation in two-layered dense mixed forests from uav lidar data. *Drones*, 4(2), 1-20. doi:10.3390/drones4020010
- Wallace, L. O., Lucieer, A., & Watson, C. S. (2012). Assessing the feasibility of UAV-based lidar for high resolution forest change detection. In *International Archives of the Photogrammetry, Remote Sensing and Spatial Information Sciences - ISPRS Archives* (pp. 499-504)
- Wang, D., Hollaus, M., Puttonen, E., & Pfeifer, N. (2016). Automatic and self-adaptive stem reconstruction in landslide-affected forests. *Remote Sensing*, 8(12). doi:10.3390/rs8120974
- Wang, Y., Lehtomäki, M., Liang, X., Pyörälä, J., Kukko, A., Jaakkola, A., Liu, J., Feng, Z., Chen, R., & Hyyppä, J. (2019). Is field-measured tree height as reliable as believed – A comparison study of tree height estimates from field measurement, airborne laser scanning and terrestrial laser scanning in a boreal forest. *ISPRS Journal of Photogrammetry and Remote Sensing*, 147, 132-145. doi:10.1016/j.isprsjprs.2018.11.008
- Watt, M. S., Meredith, A., Watt, P., & Gunn, A. (2014). The influence of LiDAR pulse density on the precision of inventory metrics in young unthinned Douglas-fir stands during initial and subsequent LiDAR acquisitions. *New Zealand Journal of Forestry Science*, 44(1), 1-9.
- Watt, P. J., & Donoghue, D. N. M. (2005). Measuring forest structure with terrestrial laser scanning. *International Journal of Remote Sensing*, 26(7), 1437-1446. doi:10.1080/01431160512331337961

- Windrim, L., & Bryson, M. (2019). Forest Tree Detection and Segmentation using High Resolution Airborne LiDAR. In *IEEE International Conference on Intelligent Robots and Systems* (pp. 3898-3904)
- Windrim, L., & Bryson, M. (2020). Detection, Segmentation, and Model Fitting of Individual Tree Stems from Airborne Laser Scanning of Forests Using Deep Learning. *Remote Sensing*, 12(9), 1469.
- Xi, Z., Hopkinson, C., & Chasmer, L. (2018). Filtering stems and branches from terrestrial laser scanning point clouds using deep 3-D fully convolutional networks. *Remote Sensing*, 10(8). doi:10.3390/rs10081215
- Zhang, W., Wan, P., Wang, T., Cai, S., Chen, Y., Jin, X., & Yan, G. (2019). A novel approach for the detection of standing tree stems from plot-level terrestrial laser scanning data. *Remote Sensing*, 11(2). doi:10.3390/rs11020211